Sub-Doppler two-photon absorption induced by the combination of a single-mode laser and a frequency comb

Marco P. Moreno
Departamento de Física, Universidade Federal de Rondônia, 76900-726 Ji-Paraná, Rondônia, Brazil

Giovana T. Nogueira
Departamento de Física, Universidade Federal de Juiz de Fora, 36036-330 Juiz de Fora, Minas Gerais, Brazil

Daniel Felinto and Sandra S. Vianna*
Departamento de Física, Universidade Federal de Pernambuco, 50670-901 Recife, Pernambuco, Brazil
(Received 14 June 2017; published 31 August 2017)

The two-photon transition $5S$-$5P$-$5D$ in rubidium vapor is investigated by detecting the fluorescence from the $6P_{3/2}$ state when the atomic system is excited by the combined action of a cw diode laser and a frequency comb. The cw laser plays a role as a velocity-selective filter and allows for sub-Doppler spectroscopy over a large spectral range including the $5D_{3/2}$ and $5D_{5/2}$ states. For a counterpropagating beam configuration, the response of each atomic velocity group is well characterized within the Doppler profile and the excited hyperfine levels are clearly resolved. The contribution of the optical pumping to the direct two-photon process is also revealed. The results are well described in a frequency domain picture by considering the interaction of each velocity group with the cw laser and the modes of the frequency comb.

DOI: 10.1103/PhysRevA.96.023430

I. INTRODUCTION

In the past two decades, mode-locked femtosecond lasers have been established as an important tool for atomic and molecular spectroscopy, with applications in the fields of biology, chemistry, and physics [1–4]. With a spectrum consisting of evenly spaced narrow lines, the phase-controlled wide-bandwidth optical frequency comb provides a precise and direct link between microwave and optical frequencies [1] and can cover from extreme UV [5] to the mid-IR [6]. In these applications, a great variety of sets of techniques have been developed, usually based on the use of the frequency comb either as a rule to measure the frequency of a cw laser, which interacts with an atomic transition [7,8], or as a single direct probe of an atomic or molecular transition [9]. Commonly, in the direct frequency comb spectroscopy, a single frequency component of the broad comb spectrum is used to selectively excite one-photon transitions [10,11], whereas for transitions of two photons, it is possible to explore the fact that the resonance condition can be simultaneously satisfied by many pairs of comb lines [12–14]. An interesting example along these lines is the recent demonstration [15] that the entire spectrum of an optical frequency comb can cool and trap atoms when used to drive a narrow two-photon transition.

In this work we focus on a different scheme, based on the introduction of a second cw laser that works in combination with the femtosecond laser so that both interact with the atomic system. In this scheme, the narrowband laser assumes the role of a velocity-selective filter, allowing a sub-Doppler spectroscopy in atomic systems where the relaxation times are longer than the repetition period and coherent accumulation processes are present [16]. Previous investigations of one-photon and two-photon transitions with this scheme have already been performed [17,18]. In the case of one-photon transition, the cw laser probes the action of the femtosecond laser over the various velocity groups, resulting in the frequency comb printed on the Doppler profile, due to the velocity distribution of the excited-state population, and in the velocity-selective population transfer between the atomic ground-state hyperfine levels [19]. When a femtosecond laser with 1-GHz frequency separation of the optical modes is applied to investigate an atomic vapor at room temperature, only one mode can fit within the Doppler profile, allowing us to distinguish the different hyperfine levels [20], similar to the traditional saturation spectroscopy. The situation is different for the two-photon transition, when the cw laser is responsible for driving one of the steps of the excitation process. In particular, for the $5S \rightarrow 5P \rightarrow 5D$ two-photon transition in rubidium vapor, previous studies using counter- and copropagating beam configurations revealed well-resolved hyperfine levels of the $5D$ state (counterpropagating beams) [18] and the frequency comb, which drives the upper transition, printed in the excitation spectra of the blue fluorescence (copropagating beams) [21]. A similar scheme [22] using the double-resonance optical pumping spectroscopy has also been applied to measure the $5P$-$4D$ transition in Rb.

Here we present an extension of our previous study on the combined action of a train of ultrashort pulses and a cw diode laser over the $5S \rightarrow 5P \rightarrow 5D$ two-photon transition in rubidium vapor [18]. Using a counterpropagating beams configuration, we explore the selectivity in the velocity and analyze the response of different groups of atoms within the Doppler profile. By setting the repetition rate of the femtosecond laser and varying the diode frequency, we probe the different groups of atoms that can interact with a fixed mode of the frequency comb. On the other hand, we can also probe a specific group of atoms each time by selecting a fixed diode frequency and scanning the repetition rate. In particular, the former scheme allows us to use the saturated

*vianna@ufpe.br

absorption signal of the diode lasers as a frequency guide inside the Doppler profile and to associate the fluorescence signal with each atomic velocity group. In addition, working with a femtosecond laser with a 1-GHz high repetition rate, the necessary condition for the accumulation of population and coherence is easily fulfilled and a good description of the results is obtained considering a three-level cascade system interacting with a cw laser and a single mode of the frequency comb.

Moreover, our results also reveal the contribution of the optical pump, induced by the diode laser, to the direct two-photon absorption process due only to the femtosecond laser. In this case, broad peaks are observed and theoretical calculations including two modes of the frequency comb are performed.

The paper is organized as follows. We introduce our experimental setup in Sec. II together with the central experimental results. In Sec. III we present our model for the experiments of Sec. II, taking into account power broadening effects. To validate our approximations in the frequency-domain treatment, we compare them with the results obtained in the time domain, considering the whole train of ultrashort pulses. We also compare the experimentally calculated responses of different atomic velocity groups and analyze the influence of the optical pumping to the fluorescence signal. We summarize in Sec. IV.

II. EXPERIMENT

Our experimental setup is schematically illustrated in Fig. 1 together with the relevant energy levels. A diode laser, stabilized in temperature and with a linewidth of about 1 MHz, is used to excite the $5S_{1/2} \rightarrow 5P_{3/2}$ transition at 780 nm. A train of femtosecond pulses generated by a mode-locked Ti:sapphire laser (BR Labs Ltda) can excite both $5S_{1/2} \rightarrow 5P_{3/2}$ and $5P_{3/2} \rightarrow 5D$ transitions. The two beams are overlapped, with orthogonal linear polarizations and in a counterpropagating configuration, in the center of a sealed Rb vapor cell. The vapor cell is heated to approximately 80 °C and contains both ^{85}Rb and ^{87}Rb isotopes in their natural abundances.

The Ti:sapphire laser produces 100-fs pulses with 12 nm of bandwidth and 300 mW of average power such that the power per mode is approximately equal to 60 μW. The $f_R = 1$ GHz repetition rate is measured with a photodiode and phase locked to a signal generator (E8663B-Agilent), with 1-Hz resolution, while the carrier-envelope-offset frequency f_{ceo} is left free. The diode laser can sweep over 10 GHz by tuning its injection current and a saturated absorption setup is used to calibrate its frequency. A direct detection of the diode-beam transmission after passing through the cell gives information about the absorption in the $5S \rightarrow 5P$ transition. The diameter of the two beams at the center of the cell is on the order of 250 μm for the femtosecond beam and 1.8 mm for the diode laser, leading to a common interaction time of about 800 ns (corresponding to a linewidth of $\gamma \approx 2\pi \times 200$ kHz).

The fluorescence at 420 nm emitted by spontaneous decay from the $6P$ state to the $5S$ is collected at 90°, using a 10-cm focal lens and a filter to cut the scattered light from the excitation laser beams. The signal is detected with a photomultiplier tube and recorded on a digital oscilloscope. Figure 2 shows the fluorescence signal (red middle curve),

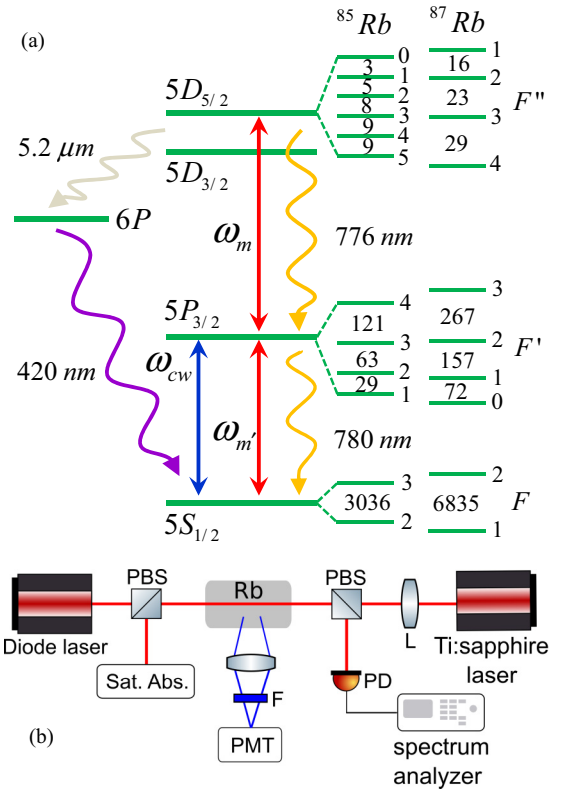

FIG. 1. (a) Schematic representation of the energy levels of Rb that are relevant for the experiment. The hyperfine splittings are in units of MHz. (b) Experimental setup, where the symbols PMT, PBS, PD, and F stand for the photomultiplier tube, polarizer beam splitter, photodiode, and filter, respectively.

for fixed f_R, as the diode frequency is scanned over the four Doppler-broadened D_2 lines of ^{85}Rb and ^{87}Rb. The spectrum consists of several narrow peaks over a flat background. The

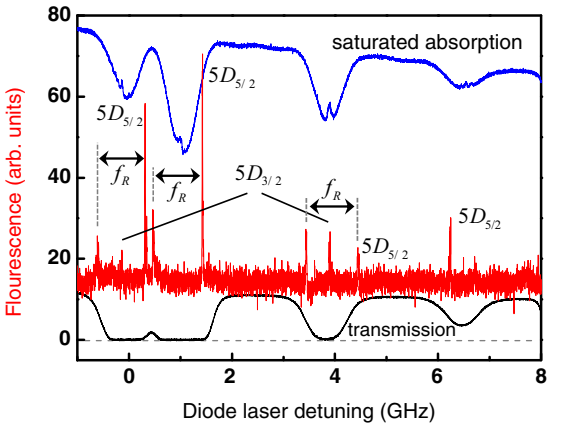

FIG. 2. Fluorescence from the $6P_{3/2} \rightarrow 5S_{1/2}$ decay as a function of the diode laser frequency for the four D_2 Doppler lines (red middle curve) with $f_R = 1.004\,411\,920$ GHz. The saturated absorption signal (blue top curve) and the diode transmission after the Rb cell (black bottom curve) are detected simultaneously with the fluorescence signal. Zero detuning is chosen at the $5S, F_g = 2 \rightarrow 5P_{3/2}, F' = 3$ transition in ^{87}Rb.

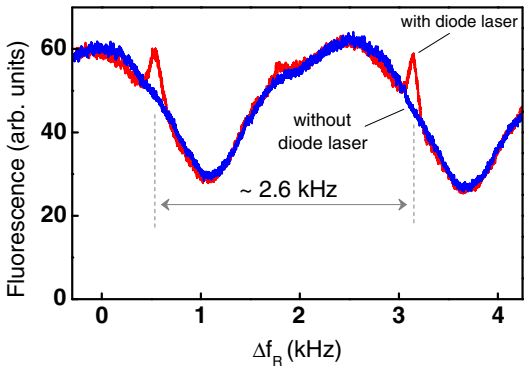

FIG. 3. The $6P_{3/2} \rightarrow 5S_{1/2}$ fluorescence as a function of femtosecond laser repetition rate variation Δf_R with and without the presence of the diode beam (tuned in the $F = 2 \rightarrow F'$ transition in ^{87}Rb).

narrow peaks are due to the two-photon transition excited by both lasers, i.e., the diode laser and the different modes of the frequency comb, while the background is due only to excitation by the frequency comb. In the same scan we can observe, simultaneously, peaks associated with the excitation of the $5D_{3/2}$ and $5D_{5/2}$ states. We also see two peaks, separated by one f_R in optical frequency of the diode laser, that correspond to the same transition excited by two neighboring modes of the frequency comb that are resonant with two different velocity groups. We also present a measurement of the direct transmission of the diode beam after passing through the warm cell (black bottom curve), indicating the strong absorption in the center of the Doppler lines. The saturated absorption curve (blue top curve) is used to calibrate the diode frequency. All the three curves are detected simultaneously.

We can also detect the fluorescence signal as a function of the repetition rate for a fixed frequency of the diode laser (free running) as shown in Fig. 3. It is interesting to observe that the relation between the optical frequency of the mth mode of the frequency comb ω_m and the repetition rate f_R is given by $\omega_m = 2\pi(f_{\text{ceo}} + mf_R)$, where f_{ceo} is the carrier-envelope-offset frequency. Then, when f_R is scanning, the optical frequency of the modes near the atomic resonance ω_0 changes according to

$$\Delta\omega_m \approx \frac{\omega_0 \Delta f_R}{f_R}. \quad (1)$$

The blue (dark gray) curve represents the fluorescence signal without the presence of the diode laser and therefore due solely to the femtosecond laser (corresponding to the background signal in Fig. 2). In this case, as the two absorbed photons are copropagated, we have a Doppler-broadened line. We see that the fluorescence signal is always present, which indicates that it is always possible to find a mode in resonance with the upper transition at the same time that another mode is at resonance with at least one Doppler line for some atomic-velocity group. Besides that, the intensity of the fluorescence varies slowly as the repetition rate changes, with an enhancement not bigger than a factor of 2 near the double-resonance condition, when the energy difference

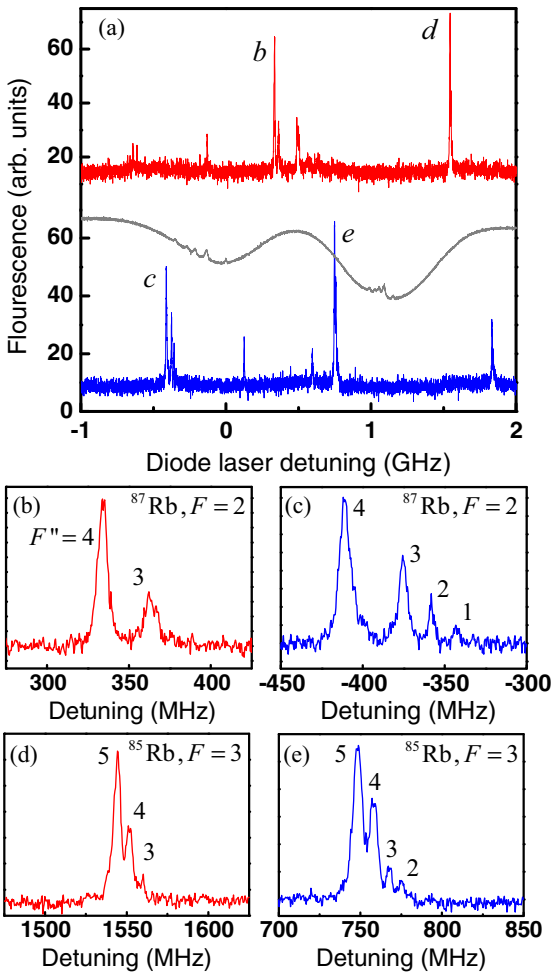

FIG. 4. (a) Fluorescence at 420 nm as a function of the diode frequency for two values of the repetition rate separated by 1800 Hz. The middle curve is the saturated absorption signal. Close-ups of the peaks are labeled on the two curves in (a) for excitation to the $5D_{5/2}$ level from the hyperfine ground states: (b) and (c) $F = 2$ of ^{87}Rb and (d) and (e) $F = 3$ of ^{85}Rb. The numbers at the peaks denote the hyperfine final state of the transitions (F'').

between two consecutive transitions is a multiple of f_R for some atomic-velocity group [23].

The red (light gray) curve in Fig. 3 represents the blue fluorescence signal now in the presence of the diode laser with a fixed frequency in one of the Doppler lines. In this case, as f_R is varied, a peak is observed when the frequency of one mode of the frequency comb plus the fixed diode frequency is equal to the frequency of the two-photon transition. From Eq. (1), this occurs at intervals of approximately $2\pi f_R^2/\omega_{5P\text{-}5D} \approx$ 2.6 kHz [23], corresponding to a change in the one-photon optical frequency of approximately 1 GHz, where $\omega_{5P\text{-}5D}$ is the frequency of the $5P_{3/2} \rightarrow 5D_{5/2}$ transition.

The fluorescence for the Doppler lines $F = 2$ of ^{87}Rb and $F = 3$ of ^{85}Rb, as a function of the diode frequency, is shown in more detail in Fig. 4. In Fig. 4(a) we compare the fluorescence signal, in the same frequency interval of the diode laser, for two values of the repetition rate, separated by 1800 Hz and with $f_R = 1.004\,411\,950$ GHz for the red top curve. The middle curve is the saturated absorption. It is clear

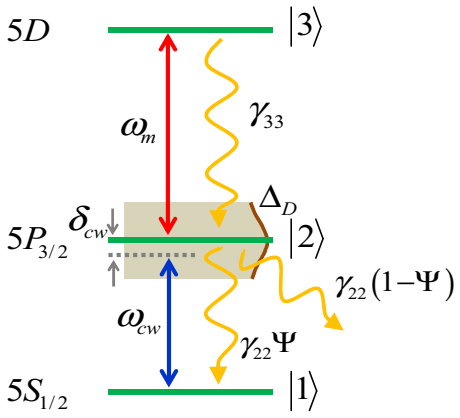

FIG. 5. Schematic representation of the cascade three-level system used to model the experimental results.

that the intensity, frequency position, and number of peaks depend of the repetition rate. This is because the frequency of the modes responsible for the upper transition changes with the repetition rate, so the peaks appear only when the diode frequency plus one mode frequency is equal to the difference in frequency between the $5S$ and $5D$ states. A close-up of each one of the four peaks labeled on the two curves in Fig. 4(a) is displayed in Figs. 4(b) and 4(c) for excitation from the hyperfine ground state $F = 2$ of ^{87}Rb and in Figs. 4(d) and 4(e) from the ground state $F = 3$ of ^{85}Rb. As we can see, each peak in Fig. 4(a) (also in Fig. 2) consists of a group of peaks, which are the result of excitation from a given ground-state hyperfine level to all the hyperfine levels (F'') of the excited state.

III. THEORY

In this section we present our theoretical model starting with the Bloch equations in Sec. III A, where we introduce the main approximations to obtain an analytical expression that will be used to describe our experimental data. The modeling and the velocity selective process are discussed in Sec. III B, along with a comparison with results obtained by numerical calculation in the time domain, considering the whole train of ultrashort pulses. In Sec. III C we investigate the influence of the optical pumping in the two-photon absorption process.

A. Bloch equations and preliminary considerations

In order to explain the experimental results presented in the preceding section we use a simple model consisting of independent three-level cascade systems interacting with the two fields as schematized in Fig. 5. We denote the hyperfine levels of the ground $(5S_{1/2}, F)$, intermediate $(5P_{3/2}, F')$, and final $(5D, F'')$ states by $|1\rangle$, $|2\rangle$, and $|3\rangle$, respectively. The cw diode laser field drives the lower transition $|1\rangle \to |2\rangle$ $(5S \to 5P_{3/2})$, with the femtosecond laser driving the upper transition $|2\rangle \to |3\rangle$ $(5P_{3/2} \to 5D)$. As we are interested in the combined action of the diode and the femtosecond lasers, we neglect the background, by assuming that the femtosecond field does not excite the transition $|1\rangle \to |2\rangle$.

The Hamiltonian of the system is given by $\hat{H} = \hat{H}_0 + \hat{H}_{\rm int}$, where $\hat{H}_0 = \hbar\omega_{21}|2\rangle\langle 2| + \hbar\omega_{32}|3\rangle\langle 3|$ represents the Hamiltonian for the free atom, with the transition frequencies $\omega_{ij} = (E_i - E_j)/\hbar$ and E_i the energy of the ith level. The coupling $\hat{H}_{\rm int}$ describing the interaction between each atom and the two lasers is

$$\hat{H}_{\rm int} = -\mu_{12}E_{\rm cw}(t)|1\rangle\langle 2| - \mu_{23}E_{\rm fs}(t)|2\rangle\langle 3| + \text{H.c.}, \quad (2)$$

where μ_{ij} is the dipole moment of the $|i\rangle \to |j\rangle$ transition and $E_{\rm cw}(t)$ and $E_{\rm fs}(t)$ are the cw and femtosecond electric fields with frequencies $\omega_{\rm cw,fs}$, described by the equations

$$E_{\rm cw}(t) = \mathcal{E}_{\rm cw}e^{i\omega_{\rm cw}t}, \quad (3)$$

$$E_{\rm fs}(t) = \sum_{n=0}^{N-1}\mathcal{E}_{\rm fs}(t - nT_R)e^{i\omega_{\rm fs}t}. \quad (4)$$

Here $\mathcal{E}_{\rm cw}$ is the cw field amplitude, $\mathcal{E}_{\rm fs}(t)$ is the pulse envelope of the femtosecond field, and $T_R = 1/f_R$ and N are the repetition period and the number of pulses.

The train of ultrashort pulses is described in the frequency domain as a frequency comb. In the limit $N \to \infty$, Eq. (4) can be written as a superposition of cw fields oscillating in phase [24]:

$$E_{\rm fs}(t) = \sum_{m=-\infty}^{\infty}\mathcal{E}_m e^{i\omega_m t}, \quad (5)$$

where $\mathcal{E}_m = f_R\tilde{\mathcal{E}}_{\rm fs}(\omega_m - \omega_{\rm fs})$ defines the amplitude of the mth mode of the frequency comb and $\tilde{\mathcal{E}}_{\rm fs}(\omega)$ is the Fourier transform of $\mathcal{E}_{\rm fs}(t)$. As an approximation, we take into account in Eq. (5) only the modes that are close to resonance with the $|2\rangle \to |3\rangle$ transitions. The Rabi frequencies for the diode laser and for each mode of the frequency comb are defined as

$$\Omega_{\rm cw} = \frac{\mu_{12}\mathcal{E}_{\rm cw}}{\hbar}, \quad (6a)$$

$$\Omega_m = \frac{\mu_{23}\mathcal{E}_m}{\hbar}. \quad (6b)$$

The Bloch equations for a group of atoms with velocity v in the rotating-wave approximation are given by

$$\dot{\rho}_{11} = -i\Omega_{\rm cw}\sigma_{12} + \text{c.c.} + \Psi\gamma_{22}\rho_{22} - \Gamma\left(\rho_{11} - \rho_{11}^{(0)}\right), \quad (7a)$$

$$\dot{\rho}_{22} = i\Omega_{\rm cw}\sigma_{12} + \text{c.c.} - \Omega_m\sigma_{23} + \text{c.c.} - (\gamma_{22} + \Gamma)\rho_{22} + \gamma_{33}\rho_{33}, \quad (7b)$$

$$\dot{\rho}_{33} = i\Omega_m\sigma_{23} + \text{c.c.} - (\Psi\gamma_{33} + \Gamma)\rho_{33} - \gamma_{33}\rho_{33}, \quad (7c)$$

$$\dot{\sigma}_{12} = [i\delta_{\rm cw} - \gamma_{12} - \Gamma]\sigma_{12} - i\Omega_m\sigma_{13} + i\Omega_{\rm cw}(\rho_{22} - \rho_{11}), \quad (7d)$$

$$\dot{\sigma}_{23} = [i\delta_m - \gamma_{23} - \Gamma]\sigma_{23} - i\Omega_{\rm cw}\sigma_{13} + i\Omega_m(\rho_{33} - \rho_{22}), \quad (7e)$$

$$\dot{\sigma}_{13} = [i(\delta_{\rm cw} + \delta_m) - \gamma_{13} - \Gamma]\sigma_{13} + i\Omega_{\rm cw}\sigma_{23} - i\Omega_m\sigma_{12}, \quad (7f)$$

where ρ_{kl} represents the element kl of the atomic density matrix and γ_{kl} represents its relaxation time. The finite interaction time due to the escape of atoms from the interaction region is accounted for by the relaxation rate Γ. This loss of atoms

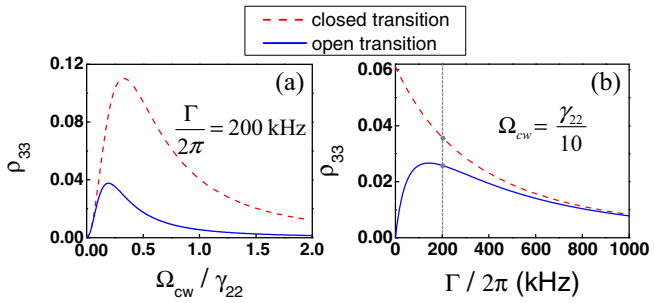

FIG. 6. Population ρ_{33} as a function of (a) the diode Rabi frequency $\Omega_{\rm cw}$ and (b) the interaction time Γ for open (blue solid curves) and closed (red dashed curves) systems in the $|1\rangle \rightarrow |2\rangle$ transition driven by the diode laser. The two fields are in resonance with their respective transitions and for both curves $\Omega_m = \gamma_{33}$.

is compensated by the arrival of new atoms in the ground state at the same rate and ρ_{11}^0 is the ground-state population in thermal equilibrium. We also consider that the $|1\rangle \rightarrow |2\rangle$ transitions, driven by the diode laser, may be closed ($\Psi = 1$) or open ($\Psi = 1/2$), depending on which F' is being excited. However, due to the longer lifetimes of the $5D$ states (resulting in weaker optical pumping) and to simplify the calculations, we consider that the $|2\rangle \rightarrow |3\rangle$ transitions are always closed.

The coherences are represented in terms of their slowly varying envelops $\sigma_{12} = \rho_{12}e^{-i\omega_{\rm cw}t}$, $\sigma_{23} = \rho_{23}e^{-i\omega_m t}$, and $\sigma_{13} = \rho_{13}e^{-i(\omega_{\rm cw}+\omega_m)t}$. The two detunings, taking into account the inhomogeneous Doppler broadening of the atomic transitions, are defined as

$$\delta_{\rm cw} = \omega_{21} - \omega_{\rm cw} - k_{\rm cw}v, \tag{8a}$$

$$\delta_m = \omega_{32} - \omega_m + k_m v, \tag{8b}$$

where $k_{{\rm cw},m}$ are the wave numbers of the cw laser and the mth mode of the frequency comb.

We assume that the blue fluorescence is proportional to the population of the state $|3\rangle$, ρ_{33}. As the diode beam may be intense, we cannot apply second-order time-dependent perturbation theory, as in Ref. [12]. The Bloch equations (7) are solved exactly in the steady-state regime, with the help of a computer algebra system.

We plot in Fig. 6 the population ρ_{33} as a function of the Rabi frequency of the diode laser [Fig. 6(a)] and the interaction time [Fig. 6(b)] for systems with the $|1\rangle \rightarrow |2\rangle$ transition open (blue solid curves) or closed (red dashed curves). In Fig. 6(a) the difference in the population for high diode laser intensities is clear, when the optical pumping becomes important. We also noticed a small difference in the values of the saturation Rabi frequency for the two systems. Figure 6(b) is another way of visualizing the distinction between them, since the ρ_{33} values are different near the region of $\Gamma/2\pi = 200$ kHz, which corresponds to the experimental conditions. The other parameters used are $\rho_{11}^0 = 1$, $\gamma_{22}/2\pi = 6$ MHz, $\gamma_{33}/2\pi = 0.66$ MHz, $\gamma_{12} = 0.5\gamma_{22}$, $\gamma_{13} = 0.5\gamma_{33}$, $\gamma_{23} = 0.5(\gamma_{33} + \gamma_{22})$, and $\Omega_m = \gamma_{33}$.

B. Modeling and velocity selectivity

To compare with the experimental spectra we need to add the contributions due to all allowed two-photon transitions ($F \rightarrow F' \rightarrow F''$):

$$\rho_{33}^{\rm calc}(\delta) = \sum_{F,F',F''} \rho_{33}^{(F,F',F'')}(\delta). \tag{9}$$

The matrix element of the electric dipole operator of each transition $F \rightarrow F'$ ($\langle F|e\hat{\mathbf{r}}|F'\rangle$) is calculated using an average over all matrix elements involving the magnetic sublevels m_F and $m_{F'}$, which are obtained by the Wigner-Eckart theorem and the Clebsch-Gordan relations [25]

$$\langle F,m_F|e\hat{r}_q|F',m_{F'}\rangle = (-1)^{2F'+I+J+J'+L+S+m_F+1}\langle L\|e\hat{\mathbf{r}}\|L'\rangle\sqrt{(2F+1)(2F'+1)(2J+1)(2J'+1)(2L+1)}$$
$$\times \begin{pmatrix} F' & 1 & F \\ m_{F'} & -q & -m_F \end{pmatrix} \begin{Bmatrix} J & J' & 1 \\ F' & F & I \end{Bmatrix} \begin{Bmatrix} L & L' & 1 \\ J' & J & S \end{Bmatrix}, \tag{10}$$

where $\langle L\|e\hat{\mathbf{r}}\|L'\rangle$ is the reduced matrix element that does not depend on the magnetic sublevels or the total angular momentum (F, F', or F'') and $\hat{r}_q$ is the q component of the vector operator $\hat{\mathbf{r}}$ in the spherical basis. The ( ) and { } terms are the 3-j and 6-j Wigner symbols, respectively.

For a specific transition $F \rightarrow F' \rightarrow F''$, we calculate the population ρ_{33} of the final F'' state, in the steady-state regime, by solving the Bloch equations for one specific diode frequency ($\delta = \delta_{\rm cw}$) integrated over the contribution of all velocity groups ($\Delta = k_{\rm cw}v$) within the Doppler profile

$$\rho_{33}^{(F,F',F'')}(\delta) = \frac{1}{\left(0.36\pi\,\Delta_D^2\right)^{1/2}} \int_{-\infty}^{\infty} \rho_{33}(\Delta,\delta;\Omega_{F,F'},\Omega_{F',F''}) \times e^{-\Delta^2/0.36\Delta_D^2} d\Delta, \tag{11}$$

with Δ_D being the inhomogeneous Doppler linewidth. In the calculations, the strength of a specific $F_i \rightarrow F_j$ transition is parametrized by the corresponding Rabi frequency $\Omega_{F_i,F_j} = (\mu_{F_i,F_j}\mathcal{E})/\hbar$, where μ_{F_i,F_j} is the electric dipole moment for the transition and in the direction of the electric field, whose amplitude $\mathcal{E}$ may refer to the diode laser $\mathcal{E}_{\rm cw}$ or a single mode of the frequency comb $\mathcal{E}_m$, depending on the transition. As we do not know the carrier-envelope-offset frequency, the frequency of the mode that drives the $F' \rightarrow F''$ transition is determined by the two-photon resonance condition combined with the diode frequency and the velocity of the atoms at resonance. For an atom with velocity v, the frequencies of the diode laser ($5S \rightarrow 5P$ transition) and of the mode m of the frequency comb ($5P \rightarrow 5D$ transition) are different, which gives a two-photon linewidth of approximately $\gamma_{33} + \gamma_{22}(\omega_m + \omega_{\rm cw})/\omega_{21}$ [26].

We assume that the two laser beams are counterpropagating, with perpendicular polarizations, as in the experiment, and calculate the population of the final state $|3\rangle$, $\rho_{33}^{(F,F',F'')}$, for each of the eight allowed two-photon transitions of ^{87}Rb,

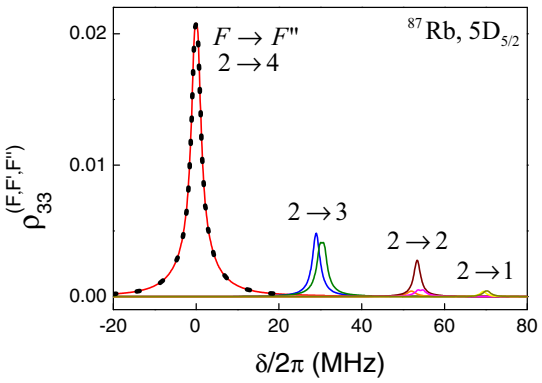

FIG. 7. (a) Population $\rho_{33}^{(F,F',F'')}$ as a function of the diode laser detuning for all allowed two-photon transitions of ^{87}Rb, starting from the Doppler line $F = 2$. We consider that the group of atoms with $v = 0$ is simultaneously in resonance with the diode laser at the $F = 2 \rightarrow F' = 3$ transition and with the mode m at the $F' = 3 \rightarrow F'' = 4$ transition. The dotted curve represents ρ_{33} for the $F = 2 \rightarrow F' = 3 \rightarrow F'' = 4$ transitions calculated via the fourth-order Runge-Kutta method.

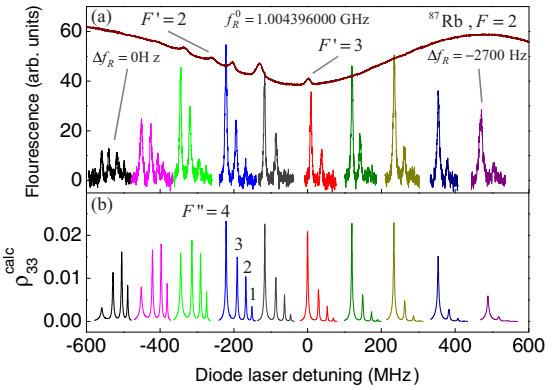

FIG. 8. (a) Curves of the fluorescence signal, for different values of repetition rate of the femtosecond laser, as the diode laser scans the ^{87}Rb, $F = 2$ line (each color corresponds to one value of the repetition rate). The top curve is the saturated absorption signal of the diode laser. (b) Excited state population ρ_{33}, calculated from Eq. (9), for the same values of the repetition rate in (a).

starting from the Doppler line $F = 2$. We consider also that the cw laser is absorbed according to the Beer law, so that its intensity varies within the Doppler profile:

$$\mathcal{E}_{\rm cw} = \mathcal{E}_{\rm cw}^0 \exp\left(-\alpha z e^{-\delta^2/0.36\Delta_D^2}\right), \tag{12}$$

where αz is the optical density and $\mathcal{E}_{\rm cw}^0$ simulates the field amplitude at the entrance of the Rb cell.

The results are shown in Fig. 7. We consider that the group of atoms with $v = 0$ is simultaneously in resonance with the diode laser at the $F = 2 \rightarrow F' = 3$ transition and with the mode m at the $F' = 3 \rightarrow F'' = 4$ transition. The integral of Eq. (11) was calculated numerically by considering $\Delta_D/2\pi = 590$ MHz and the values of the field amplitudes, obtained from the experimental conditions, were $\mathcal{E}_{\rm cw}^0 = 350$ V/m ($\Omega_{\rm cw} \approx 2.7\gamma_{22}$ at $F = 2 \rightarrow F' = 3$) and $\mathcal{E}_m = 350$ V/m ($\Omega_m \approx 6.6\gamma_{33}$ at $F' = 3 \rightarrow F'' = 4$). The diode beam absorption was considered by assuming $\alpha z = 1.5$. As the two absorbed photons do not have the same frequency, different group of atoms are excited depending of the intermediate pathway. An example is the two peaks, almost superimposed, labeled by $2 \rightarrow 3$ in Fig. 7 (blue and green curves), corresponding to the transitions $F = 2 \rightarrow F' = 3 \rightarrow F'' = 3$ and $F = 2 \rightarrow F' = 2 \rightarrow F'' = 3$. The frequency difference for these two transitions is on the order of $\delta_{F'} = 1.4$ MHz and is given by the general expression [26]

$$\delta_{F'} = \triangle_{F'}\left(\frac{\lambda_{\rm cw}}{\lambda_m} - 1\right), \tag{13}$$

where $\triangle_{F'}$ is the frequency difference between the two hyperfine levels F' that participate in each pathway.

In fact, the greatest contribution for the upper level population ρ_{33} comes from the closed transition $F = 2 \rightarrow F' = 3 \rightarrow F'' = 4$. We use this transition to analyze the response of the system obtained in the time domain, considering the train of pulses given by Eq. (4). In this case, the Bloch equations are numerically solved in time by the classical fourth-order Runge-Kutta method, for each diode frequency and for each atomic group velocity. As this computation is very time consuming, we calculated the density-matrix elements for all atomic group velocities in parallel using multiple threads of a graphic processing unit [27]. In this case, we have considered $N = 1000$ pulses, $T_R = 1$ ns, $T_p = 100$ fs (temporal linewidth of the pulses), and $\mathcal{E}_{\rm fs}(0) = 3.5 \times 10^6$ V/m. The response from the time domain calculations is represented by the black dots in Fig. 7, which appears over the curve labeled by $2 \rightarrow 4$ (red curve) obtained from the frequency domain calculations. The agreement between the two results is excellent and indicates how good the approximation of working with a single mode of the frequency comb is under the condition $\gamma_{33} \ll f_R$. In the time domain, we can interpret this fact as due to the coherent accumulation process, in the upper transition, determined by constructive and destructive interferences between the electric field of the train of pulses and the coherence excited by it. In particular, under the high repetition rate of the femtosecond laser, 1 GHz, the necessary condition for the coherent accumulation of population and coherence is fulfilled much better.

Another interesting feature is the strong dependence of the intensity relation between the peaks showed in Fig. 7 ($F = 2 \rightarrow F''$) on the atomic-velocity group that participates in the two-photon transition. This dependence can be seen in Fig. 8, where we compare theory and experiment for the fluorescence signal of the ^{87}Rb, $F = 2$ line. We plot, in the same picture [Fig. 8(a)], several curves corresponding to the fluorescence signal obtained for different values of the repetition rate, as a function of the diode laser detuning. For a better comparison we subtracted the signal due only to the femtosecond laser (background). The top curve is the saturated absorption signal of the diode laser and is the same for all fluorescence signals of the picture. The first fluorescence curve on the left (the black set of peaks) was obtained for $f_R = f_R^0 = 1.004\,396\,000$ GHz ($\triangle f_R = 0$). In this case, we can see four peaks corresponding to the four possible hyperfine levels F'' that can be excited starting from $F = 2$, all with almost the same intensity. As we vary the repetition rate ($\triangle f_R = 300$ Hz) other atomic-velocity groups will be at resonance, so the corresponding fluorescence

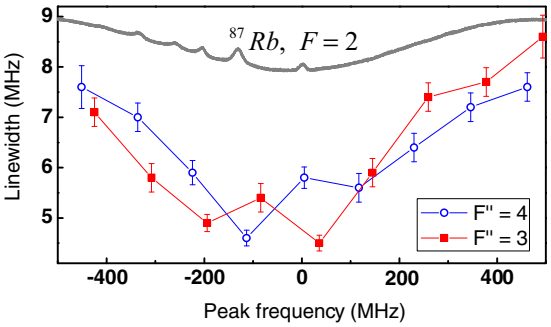

FIG. 9. Average linewidth of the peaks corresponding to the $F = 2 \rightarrow F'' = 3$ (squares) and $F = 2 \rightarrow F'' = 4$ (open circles) transitions as a function of their position within the Doppler profile. The top curve is the saturated absorption curve of the diode laser.

curve (the magenta set of peaks) will appear at a different diode frequency, dislocated in the saturated absorption curve. The variation of $\triangle f_R$ between the curves is of 300 Hz and the total variation ($\triangle f_R = 2700$ Hz) corresponds to a change in the optical diode frequency of almost 1 GHz.

The hyperfine levels of the intermediate state $5P_{3/2}$ have a strong influence on this intensity relation between the peaks. As we saw in Fig. 7, depending of the final level F'', different hyperfine levels F' can contribute for the same two-photon peak. For example, the resonant two-photon transition $F = 2 \rightarrow F'' = 4$ involves only one pathway ($F = 2 \rightarrow F' = 3$), whereas the transition $F = 2 \rightarrow F'' = 3$ has the contribution of two pathways ($F = 2 \rightarrow F' = 2,3$). In addition to the influence of the value of the electric dipole moment, we know that the more atoms are being excited, the greater the peak amplitude of the two-photon transition. This behavior is in agreement with the results showed in Fig. 8(a), since on the left side of the Doppler curve, the transitions $F = 2 \rightarrow F'' = 1,2$, with smaller electric dipole moment, are in resonance with more group of atoms (near the frequency transition $F = 2 \rightarrow F' = 1,2$ with the diode laser), making possible the observation of the four peaks. However, on the right side of the Doppler curve these transitions are far apart and so these peaks do not appear.

In Fig. 8(b) we plot the excited-state population ρ_{33}, calculated from Eq. (9), as a function of the diode laser detuning, for the same values of the repetition rate presented in Fig. 8(a). In this modeling the values of the electric field of the two lasers were calculated from the power measured during the experiment. As we can see, our theoretical model not only describes well the intensity relation between the peaks for the same atomic-velocity group but also gives a good intensity relation between peaks of different atomic-velocity groups. The description is better near the center of the Doppler line where the contribution for the excitation process is predominantly due to atoms with $v = 0$. The discrepancy is mainly on the sides of the Doppler line, where the experimental peaks present a small broadening. The average linewidth of the peaks corresponding to the $F = 2 \rightarrow F'' = 3,4$ transitions as a function of their position within the Doppler profile is displayed in Fig. 9. At the center, the diode power is on the order of μW ($\mathcal{E}_{cw} \approx 100$ V/m), due to the strong absorption of the diode beam near the resonance, giving a linewidth around 5 MHz, whereas on the sides of the Doppler profile the linewidth tends to almost 10 MHz, indicating a power broadening contribution. Other effects that also contribute to the broadening are (i) the linewidth of the diode laser (∼1 MHz), (ii) the jitter of the offset frequency in one scan, (iii) the Zeeman sublevels, and (iv) the broadening due to the time response of the photomultiplier. All these effects were not taken into account in our theoretical model.

C. Influence of the optical pumping

An interesting situation occurs when one group of atoms is in resonance, simultaneously, with an one-photon transition, driven by the diode laser, and with a two-photon transition, driven only by the femtosecond laser. In this case, the optical pumping induced by the diode laser can contribute to an increase or decrease of the background signal of the blue fluorescence, which is only due to the two-photon transition by the femtosecond mode-locked laser. An example of this effect is shown in Fig. 10, where the bottom curve represents the fluorescence signal as a function of the diode laser frequency detuning for an average of ten scans processed by the oscilloscope. We clearly see two broad peaks, with linewidths on the order of 29 and 44 MHz, respectively, separated by ∼157 MHz, which are due to the optical pumping by the diode laser. For these conditions, one of the peaks corresponds to the fluorescence of a group of atoms that is in resonance, simultaneously, with the diode laser at the one-photon transition $F = 2 \rightarrow F' = 2$ and with the femtosecond laser at $F = 1 \rightarrow F''$ two-photon transition, whereas the other large peak comes from the other group of atoms that is in resonance with the diode laser at the $F =$

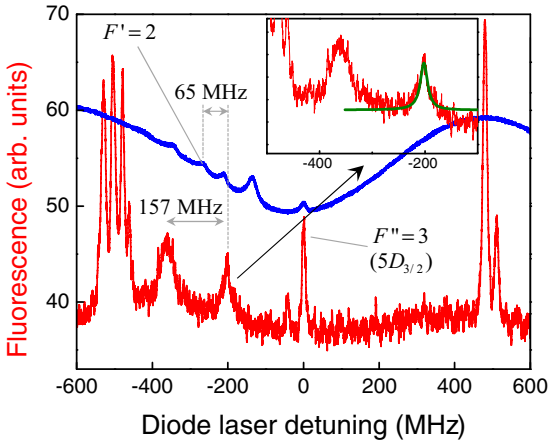

FIG. 10. (a) Fluorescence at 420 nm as a function of the diode laser detuning for the ^{87}Rb, $F = 2$ line (red bottom curve). The narrow peaks in the center and the sides correspond to the transitions $5S_{1/2} \rightarrow 5D_{3/2}$ and $5S_{1/2} \rightarrow 5D_{5/2}$, respectively. The broad peaks indicated by a separation of 157 MHz are those induced by the diode optical pumping. The curve is an average of ten scans. The top blue curve is the saturated absorption. For this scan $f_R = 1.004\,382\,780$ GHz and $f_{ceo} = 692$ MHz (see the text). The green solid line in the inset is the calculated ρ_{33} population, using $\mathcal{E}^0_{cw} = 500$ V/m, $\mathcal{E}_m = 350$ V/m, and $\mathcal{E}_{m'} = 400$ V/m.

$2 \rightarrow F' = 1$ transition (separated by 157 MHz from the other transition).

The Bloch equations (7) can also be used to model the shape of the peaks induced by optical pumping. For this we need to take into account two modes m and m' of the frequency comb, in a copropagating configuration, and consider that the cw field of the diode laser contributes only to modify the population of state $|1\rangle$. A schematic representation of the energy levels is shown in Fig. 11. The $|a\rangle$ and $|b\rangle$ states are not included in the Bloch equations and they are only used to describe the ground-state population changes due to the optical pumping. Thus we solve Eqs. (7), replacing the field of the cw laser by the field of the m'th mode and the ground-state population

$$\rho_{11}^{(0)} \rightarrow \rho_{11}^{(0)} + \left[1 + \frac{\gamma_{bb}^2 + 4\left(\Omega_{\rm cw}^2 + \delta_{\rm cw}^2\right)}{2\Omega_{\rm cw}^2(\gamma_{bb}/\Gamma)}\right]^{-1}. \tag{14}$$

The second term on the right-hand side of Eq. (14) is the solution of the Bloch equations in the steady-state regime for ρ_{11} in a Λ-type three-level system ($|a\rangle$, $|b\rangle$, and $|1\rangle$, Fig. 11) when the cw laser is close to the $|a\rangle \rightarrow |b\rangle$ transition in the approximation $\Gamma \ll \Omega_{\rm cw}, \gamma$ [20]. The position of these large peaks into the Doppler profile also influences their shapes and can be determined from f_R, $f_{\rm ceo}$, and the detunings of the one- and two-photon resonances.

Although we have not measured the offset frequency of the femtosecond laser we can estimate its value, for a set of scans, by using the frequency values of the atomic transitions that are very well known. For that we select a peak in the blue fluorescence signal related to a specific two-photon transition and use the fact that this signal is generated by a specific group of atoms that satisfy the resonant conditions, for one and two photons, given by Eqs. (8) with $\delta_{\rm cw} = \delta_m = 0$. For the experimental curve in Fig. 10, the offset frequency is calculated from the central peak, where a group of atoms with $v = 0$ is at resonance with the diode laser in the $F = 2 \rightarrow F' = 3$ transition and with the mth mode of the frequency comb in the $F' = 3 \rightarrow F'' = 3$ ($5D_{3/2}$) transition (ω_{32}), and from the repetition rate of the femtosecond laser, $f_R = 1.004\,382\,780$ GHz,

$$f_{\rm ceo} = \frac{\omega_{32}}{2\pi} - \left\lfloor \frac{\omega_{32}}{2\pi f_R} \right\rfloor f_R, \tag{15}$$

given a value of $f_{\rm ceo} = 692$ MHz. The symbol $\lfloor\,\rfloor$ represents the integer part of a number.

In the inset of Fig. 10, the green solid line over the experimental curve represents the population ρ_{33} calculated, as in Fig. 7, with the modifications described above. From this procedure we obtain the background signal, determined by the two-photon transition driven by the modes of the frequency comb due to the interaction with the groups of atoms that are far off-resonance with the diode laser. We conclude, from the position of the broad peak with respect to the Doppler profile and from the estimated value of $f_{\rm ceo}$, that the main contributions comes from the ^{87}Rb, $F = 1 \rightarrow F' = 0 \rightarrow F'' = 1$ ($5D_{5/2}$) transitions with the modes m and m' and $F = 2 \rightarrow F' = 2$ with the cw field, having the detuning of the one-photon transition of $\epsilon/2\pi = -35$ MHz for the atomic-velocity group at 65 MHz.

In the approximation of $\Gamma_{\rm cw} \ll \Omega_{\rm cw}, \gamma_{bb}$, Eq. (14) gives a linewidth of

$$\triangle\omega = \Omega_{\rm cw}(2\gamma_{bb}/\Gamma_{\rm cw})^{1/2}. \tag{16}$$

From Eq. (16) we get $\triangle\omega/2\pi = 15$ MHz, less than the experimental linewidth (29 MHz). As f_R is fixed, the main mechanism that increases the peak linewidth is the fluctuation during the average of ten scans, caused mainly by the free carrier-envelope-offset frequency $f_{\rm ceo}$.

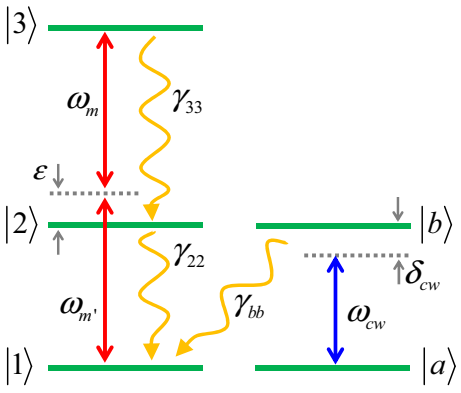

FIG. 11. (a) Theoretical model to describe the peaks induced by the diode optical pump. States $|a\rangle$ and $|b\rangle$ (not included in the Bloch equations) are used in Eq. (14) to modify the population of state $|1\rangle$. Here ϵ represents the detuning of the modes m and m' in relation to the transition with the intermediate level.

IV. CONCLUSION

In this paper we have presented results on the sub-Doppler two-photon absorption induced by the combined action of a single-mode laser and a frequency comb. The blue fluorescence was investigated when the cw-laser frequency, at a fixed repetition rate of the femtosecond laser, is scanned over the D_2 Doppler lines of ^{85}Rb and ^{87}Rb, showing a large spectral range that includes the $5D_{3/2}$ and $5D_{5/2}$ states. The resolution is limited by the free-running offset frequency and the linewidth of the diode laser, without the need of direct spectral filtering of the femtosecond laser. By varying the value of the repetition rate we were able to study the response of different atomic-velocity groups. Moreover, a large frequency separation of 1 GHz of the modes of the frequency comb allowed us to distinguish the hyperfine levels of the $5D$ excited state and their relative intensities for different atomic groups within the Doppler profile. A good quantitative description of the experimental spectra at different positions of the Doppler line was provided in the frequency domain picture, taking into account the high intensity and the absorption of the diode laser as well as the Maxwell-Boltzmann population distribution. We have also shown that the results of the numerical solution of the Bloch equations for a three-level system interacting with both a cw laser and the whole train of ultrashort pulses fits well our experimental data and confirm our analytical treatment

based on a single mode of the frequency comb. Further, our results also revealed the contribution of the optical pumping to the two-photon transition driven only by the femtosecond laser, which is well described by considering the interaction of the atomic system with two modes of the frequency comb. In conclusion, our work shows that the combined action of a single-mode laser and a frequency comb is a very effective tool to drive two-photon transitions efficiently and with high spectral resolution.

ACKNOWLEDGMENT

This work was supported by the following Brazilian agencies: the National Council for Scientific and Technological Development (CNPq), the Fundação de Amparo à Ciência e Tecnologia do Estado de Pernambuco (FACEPE/PRONEX), the Coordenação de Aperfeiçoamento de Pessoal de Nível Superior (CAPES), and the Fundação de Amparo à Ciência e Tecnologia do Estado de Rodônia (FAPERO).

[1] T. Udem, R. Holzwarth, and T. W. Hänsch, Optical frequency metrology, Nature (London) **416**, 233 (2002).

[2] J. Ye and S. Cundiff, *Femtosecond Optical Frequency Comb Technology: Principle, Operation and Application* (Springer, New York, 2005).

[3] A. Pe'er, E. A. Shapiro, M. C. Stowe, M. Shapiro, and J. Ye, Precise Control of Molecular Dynamics with a Femtosecond Frequency Comb, Phys. Rev. Lett. **98**, 113004 (2007).

[4] A. Nishiyama, K. Nakashima, A. Matsuba, and M. Misono, Doppler-free two-photon absorption spectroscopy of rovibronic transition of naphthalene calibrated with an optical frequency comb, J. Mol. Spectrosc. **318**, 40 (2015).

[5] R. K. Altmann, S. Galtier, L. S. Dreissen, and K. S. E. Eikema, High-Precision Ramsey-Comb Spectroscopy at Deep Ultraviolet Wavelengths, Phys. Rev. Lett. **117**, 173201 (2016).

[6] M. Vainio and J. Karhu, Fully stabilized mid-infrared frequency comb for high-precision molecular spectroscopy, Opt. Express **25**, 4190 (2016).

[7] T. Udem, J. Reichert, R. Holzwarth, and T. W. Hänsch, Absolute Optical Frequency Measurement of the Cesium D_1 Line with a Mode-Locked Laser, Phys. Rev. Lett. **82**, 3568 (1999).

[8] H.-C. Chui, M.-S. Ko, Y.-W. Liu, J.-T. Shy, J.-L. Peng, and H. Ahn, Absolute frequency measurement of rubidium 5*S*-7*S* two-photon transitions with a femtosecond laser comb, Opt. Lett. **30**, 842 (2005).

[9] A. Marian, M. C. Stowe, J. R. Lawall, D. Felinto, and J. Ye, United time-frequency spectroscopy for dynamics and global structure, Science **306**, 2063 (2004).

[10] V. Gerginov, C. E. Tanner, S. A. Diddams, A. Bartels, and L. Hollberg, High-resolution spectroscopy with a femtosecond laser frequency comb, Opt. Lett. **30**, 1734 (2005).

[11] D. C. Heinecke, A. Bartels, T. M. Fortier, D. A. Braje, L. Hollberg, and S. A. Diddams, Optical frequency stabilization of a 10 GHz Ti:sapphire frequency comb by saturated absorption spectroscopy in ^{87}rubidium, Phys. Rev. A **80**, 053806 (2009).

[12] J. E. Stalnaker, V. Mbele, V. Gerginov, T. M. Fortier, S. A. Diddams, L. Hollberg, and C. E. Tanner, Femtosecond frequency comb measurement of absolute frequencies and hyperfine coupling constants in cesium vapor, Phys. Rev. A **81**, 043840 (2010).

[13] I. Barmes, S. Witte, and K. S. E. Eikema, High-Precision Spectroscopy with Counterpropagating Femtosecond Pulses, Phys. Rev. Lett. **111**, 023007 (2013).

[14] A. Hipke, S. A. Meek, T. Ideguchi, T. W. Hänsch, and N. Picqué, Broadband Doppler-limited two-photon and stepwise excitation spectroscopy with laser frequency combs, Phys. Rev. A **90**, 011805 (2014).

[15] A. M. Jayich, X. Long, and W. C. Campbell, Direct Frequency Comb Laser Cooling and Trapping, Phys. Rev. X **6**, 041004 (2016).

[16] D. Felinto, C. A. C. Bosco, L. H. Acioli, and S. S. Vianna, Coherent accumulation in two-level atoms excited by a train of ultrashort pulses, Opt. Commun. **215**, 69 (2003).

[17] D. Aumiler, T. Ban, H. Skenderović, and G. Pichler, Velocity Selective Optical Pumping of Rb Hyperfine Lines Induced by a Train of Femtosecond Pulses, Phys. Rev. Lett. **95**, 233001 (2005).

[18] M. P. Moreno, G. T. Nogueira, D. Felinto, and S. S. Vianna, Two-photon transitions driven by a combination of diode and femtosecond lasers, Opt. Lett. **37**, 4344 (2012).

[19] D. Aumiler, T. Ban, N. Vujičić, S. Vdović, H. Skenderović, and G. Pichler, Characterization of an optical frequency comb using modified direct frequency comb spectroscopy, Appl. Phys. B **97**, 553 (2009).

[20] M. P. Moreno and S. S. Vianna, Femtosecond 1 GHz Ti:sapphire laser as a tool for coherent spectroscopy in atomic vapor, J. Opt. Soc. Am. B **28**, 2066 (2011).

[21] F. A. Lira, M. P. Moreno, and S. S. Vianna, Observing the optical frequency comb in the blue fluorescence of rubidium vapor, J. Phys. B **48**, 245001 (2015).

[22] H. S. Moon, H. Y. Ryu, S. H. Lee, and H. S. Suh, Precision spectroscopy of Rb atoms using single comb-line selected from fiber optical frequency comb, Opt. Express **19**, 15855 (2011).

[23] N. Vujičić, T. Ban, G. Kregar, D. Aumiler, and G. Pichler, Velocity-selective double resonance in Doppler-broadened rubidium vapor, Phys. Rev. A **87**, 013438 (2013).

[24] M. P. Moreno and S. S. Vianna, Comparative analysis in the frequency domain of the resonant interaction between an ultrashort pulse train and a two-level system, Opt. Commun. **313**, 113 (2014).

[25] A. R. Edmonds, *Angular Momentum in Quantum Mechanics* (Princeton University Press, Princeton, 1960).

[26] J. E. Bjorkholm and P. F. Liao, Line shape and strength of two-photon absorption in an atomic vapor with a resonant or nearly resonant intermediate state, Phys. Rev. A **14**, 751 (1976).

[27] G. Demeter, Solving the Maxwell-Bloch equations for resonant nonlinear optics using GPUs, Comput. Phys. Commun. **184**, 1203 (2013).